RSC Advances

REVIEW

View Article Online
View Journal | View Issue

Cite this: *RSC Adv.*, 2018, **8**, 19895

Adsorptive environmental applications of MXene nanomaterials: a review

Yujuan Zhang, *[a] Lin Wang, [b] Ningning Zhang[a] and Zhangjian Zhou[a]

Received 10th April 2018
Accepted 14th May 2018

DOI: 10.1039/c8ra03077d

rsc.li/rsc-advances

Since titanium carbide Ti_3C_2 nanosheets were first produced in 2011, an increasing number of members of this new family of two-dimensional transition metal carbides/nitride (MXene) materials have been successfully synthesized. Due to their large specific surface area, hydrophilic nature and abundant highly active surface sites, MXenes have been demonstrated to adsorb a variety of environmental pollutants, including heavy metal ions, organic dyes, radionuclides, and gas molecules, and thus can be used for the removal of pollutants and even sensing. In this review, we summarize the recent research progress on MXene materials in the adsorptive remediation of environmental pollutants and highlight the main challenges in the future to understand the full potential of MXene materials in environmental systems.

1 Introduction

With the development of industrialization, environmental pollution has become increasingly serious worldwide, which poses serious effects on human health and the ecosystem. The most commonly encountered pollutants include heavy metal ions, organics, bio-toxins, and toxic gases. Thus, various physical, chemical and biological techniques have been developed to remedy pollutants, such as membrane filtration, precipitation, adsorption, solvent extraction, and ion exchange.[1–4] Among them, adsorption is considered to be promising due to its simple, cost-effective and economical characteristics.[1,5] Additionally, adsorption also avoids secondary pollution due to the production of harmful substances during remediation. For effective adsorption, adsorbents usually have a large specific surface area and proper functionalities for the adsorbates. To date, numerous porous materials have been developed as adsorbents for environmental pollutants, such as activated carbon, kaolinite, zeolites, chitosan, and metal–organic frameworks.[6–11]

Two dimensional (2D) materials have garnered great attention owing to their unique physical and chemical properties, which differ from their corresponding bulk counterparts, since graphene was first produced by mechanical exfoliation into

[a]School of Materials Science and Engineering, University of Science and Technology Beijing, 100083, Beijing, China. E-mail: zhangyujuan@ustb.edu.cn
[b]Laboratory of Nuclear Energy Chemistry and Key Laboratory for Biomedical Effects of Nanomaterials and Nanosafety, Institute of High Energy Physics, Chinese Academy of Sciences, 100049, Beijing, China

Dr Yujuan Zhang is a Lecturer and Research Scientist at the University of Science & Technology Beijing (USTB). She received her PhD in Theoretical Physics from the Chinese Academy of Engineering Physics in 2013 and accomplished her postdoc work at the Institute of High Energy Physics, Chinese Academy of Sciences in 2015. Subsequently, she joined the School of Materials Science and Engineering of USTB. She was a visiting scholar to New York State University at Buffalo from Feb. 2017 to Feb. 2018. Her current research interests include simulations and predictions of novel properties of low dimensional materials.

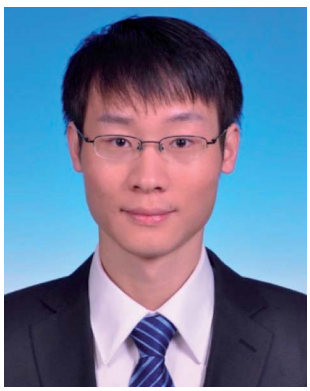

Dr. Lin Wang received his B.S. in Chemistry and PhD in Physics from Peking University in 2007 and 2012, respectively. Subsequently, he joined the Key Laboratory of Nuclear Radiation and Nuclear Energy Technology, Institute of High Energy Physics (IHEP), Chinese Academy of Sciences as a Research Assistant. He is currently an associate professor at the IHEP. His research interests include the separation of actinides by solid phase extraction and the synthesis of actinide nanomaterials.

single-layers in 2004.[12] Since the emergence of graphene, other 2D materials such as transition metal dichalcogenides (TMDs), hexagonal boron nitrides, metal oxides and hydroxides have been discovered and demonstrated in diverse applications.[13–15] As is known, low-dimensional materials with the advantage of large surface areas have been considered as ideal adsorbents for various pollutants, *e.g.*, ordered mesoporous silica, carbon-based nanomaterials (*e.g.*, carbon nanotubes and graphene), and phosphorenes.[16–20]

Recently, a new family of 2D transition metal carbide/nitride materials known as MXene has been attracting tremendous interest from both theoretical and experimental physicists and chemists.[21–26] Due to their unique structures, MXenes usually exhibit excellent properties such as high chemical stability, high electrical conductivity and environment-friendly characteristics. To date, MXenes have been reported as promising materials for application in semiconductors, hydrogen storage, supercapacitors, and lithium-ion batteries.[27–34] Especially, their hydrophilic nature and abundant highly active functional sites on their surface render MXenes effective adsorbents for many molecular or ionic species, which consequently can be used for environmental pollutant purification or even sensing. Although several review papers on MXenes have been published,[22,31–34] they generally cover all the application aspects of MXenes, and a special review on the progress of the application of MXenes in the environmental remediation area has not been reported to date. Herein, based on this fact, we focus and summarize in detail the recent research progress on MXene materials in the application of adsorptive remediation of environmental pollutants, including heavy metal ions, organic dyes, radionuclides and gaseous contaminants, and highlight the main challenges in the future to understand the full potential of MXene materials in environmental systems.

2 Structures and surface terminations of MXenes

The structure of a bare MXene can be described as n+1 layers of transition metal elements M covering n layers of X (where, X is C or N element.) in an $(MX)_nM$ arrangement. As shown in Fig. 1a, to date, at least three different formulae of MXenes, M_2X, M_3X_2 and M_4X_3,[22] have been confirmed. From the scanning electron microscope (SEM) images in Fig. 1b, the layered structures of MXenes are obvious. In addition, MXenes with two different transition metals have also been synthesized, which exist in two forms, *i.e.*, solid solution phase (two transition metals randomly occupy the M-sites) and ordered phase (two transition metals are arranged layer by layer).[31] For example, $(Cr_2V)C_2$ has an ordered structure, while (Ti and $V)_3C_2$ exist in solid solution.

Due to the important role of the specific surface area of MXene materials, the quality of MXene materials is a critical factor in environmental applications. In recent years, many preparation techniques have been developed to obtain high-quality flake nanomaterials. MXenes were first synthesized *via* a simple chemical etching method in 2011, where the "A" laminar component is exfoliated from the "MAX" matrix phase in hydrofluoric acid (HF), ammonium bifluoride (NH_4HF_2) or hydrochloric acid (HCl) combined with lithium fluoride (LiF), followed by sonication at room temperature,[22,26] as shown in Fig. 1c. The term "MAX" represents the chemical composition of the parent compounds $M_{n+1}AX_n$ (n = 1, 2 and 3), where A stands for a group IIIA or IVA element (A = Al, Ga, In, Si, Ge, Sn, Pb, P, As, S and Cd). Recently, MXenes have also been synthesized from the laminated phase, which are categorized as derivatives of MAX phases (d-MAX). For example, Zr_3C_2 and Hf_3C_2 MXenes can be synthesized *via* the selective etching of Al–C and Si-alloyed Al–C sublayers from nanolaminated $Zr_3Al_3C_5$ and $Hf_3[Al(Si)]_4C_6$, respectively.[35,36] Fig. 2 shows a schematic illustration of the synthesis of Hf_3C_2 MXene from the nanolaminated d-MAX phase $Hf_3[Al(Si)]_4C_6$. During the etching process, the introduction of Si can significantly accelerate the etching of the layered ternary carbide $Hf_3Al_4C_6$ through the weakened interfacial adhesion between the Hf–C and Al(Si)–C sublayers, as shown in Fig. 2c and d.

Surface functionalities are strongly relevant to the physical and chemical properties of MXene materials, which further affect their environmental applications. In various etching synthetic procedures, chemical functional groups such as oxygen (–O), hydroxyl (–OH) and fluorine (–F) often form on the surfaces of MXenes. Therefore, MXenes are generally written as $M_{n+1}X_nT_x$, where T refers to the surface terminated functional groups. For example, Ti_3C_2 MXene can have at least three formulae: $Ti_3C_2(OH)_2$, $Ti_3C_2O_2$ and $Ti_3C_2F_2$. In practice, Ti_3C_2 MXene usually has a combination of these functional groups, the specific quantities of which are highly dependent on the synthetic methods.[37,38] The random distribution of terminations on the surface of MXene has been confirmed by neutron scattering and NMR spectroscopy.[38,39] In general, a hydrophilic surface is beneficial for the adsorption of polar or ionic species. It is shown that the –F group is not desirable when MXenes are used for adsorbents in most circumstances, which will be discussed in the following section. Fortunately, the –O and –OH groups are found to be more stable, and –F terminations will be replaced by OH groups upon rinsing and/or storage in water. Thus, most of the terminations of MXenes obtained using the chemical etching method are –OH and –O groups.[40] This is probably why MXenes always exhibit very high adsorption capacities (in the unit of grams of adsorbate per gram of adsorbent) even compared to carbon-based nanomaterials, such as graphene, though the atomic weight of transition metal elements is usually large.

Recently, bare Mo_2C MXene without functional groups has been successfully synthesized using the chemical vapor deposition method.[41] The excellent physical properties of bare Mo_2C MXene have also been systematically explored using density functional theory (DFT).[42] The unterminated metallic atoms are considered to be highly active and easy to react with other substances. However, studies about the adsorption behaviors of MXenes without functional groups are scarce, and still need to be further studied.

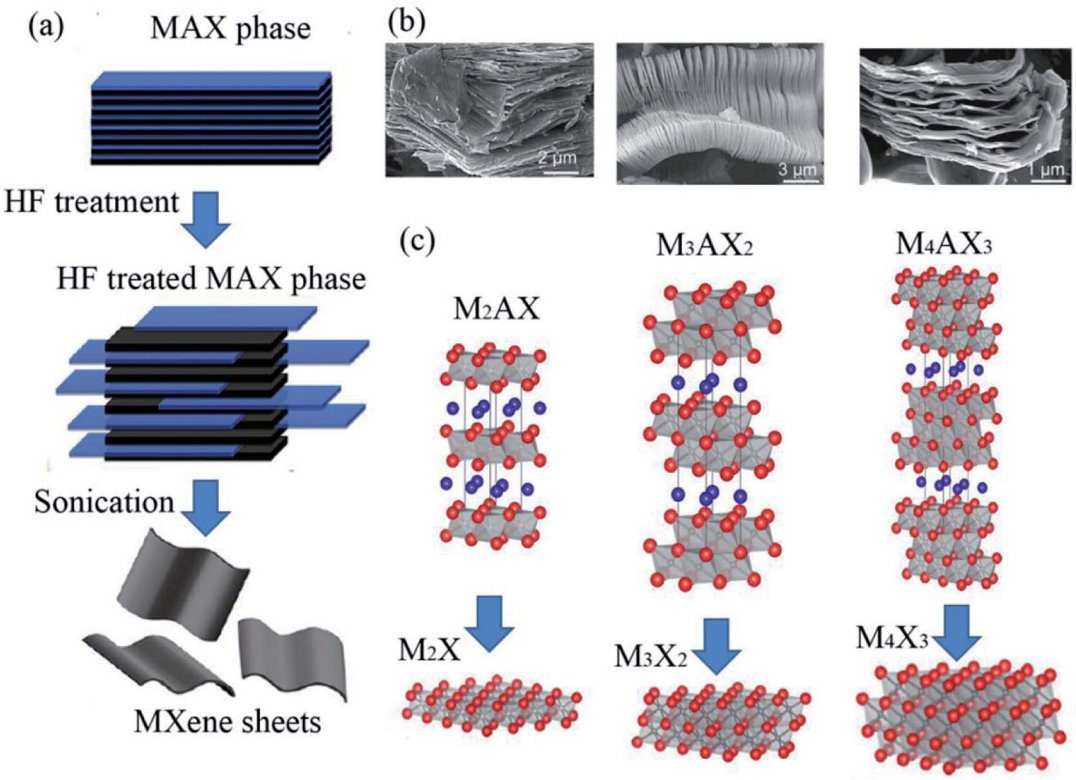

Fig. 1 (a) Early reported three different structures of MXenes (non-terminated): M_2X, M_3X_2 and M_4X_3. Reprinted from ref. 22 and 23 with permission. (b) SEM images of Ti_2AlC, Ti_3AlC_2 and Ta_4AlC_3 after HF treatment (from right to left). (c) Schematic illustration of the synthesis of MXenes from MAX phases. Copyright 2013 John Wiley and Sons and Copyright 2012 American Chemical Society.

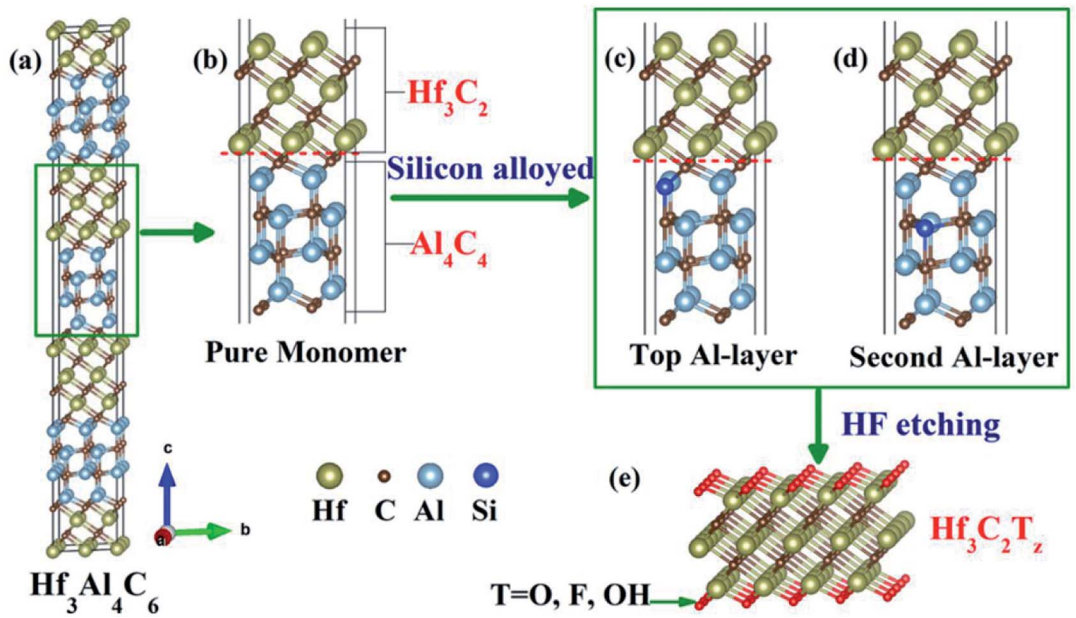

Fig. 2 Schematic illustration of the synthesis of $Hf_3C_2T_z$ MXene from nanolaminated phase $Hf_3[Al(Si)]_4C_6$. (a) Structure of $Hf_3Al_4C_6$, (b) structure of pure $Hf_3Al_4C_6$ monomer, (c) and (d) structure of two $Hf_3Al_4C_6$ monomers with different silicon alloying, and (e) side view of Hf_3C_2 MXene. Reprinted with permission of ref. 36 Copyright 2017 American Chemical Society.

3 Progress of MXenes in adsorption remediation of pollutants

3.1 Heavy metal ion adsorption

Heavy metal ions including Pb(II), Cr(IV), Hg(II), Cd(II) and Cu(II) are the most important pollutants in water and soil because of their high toxicity to humans and other living organisms. Adsorption is considered to be the most effective approach to remove heavy metal ions because other methods such as biological processes or chemical reactions cannot degrade them. Due to the abundant active sites on their surface, MXenes can adsorb metal ions through electrostatic and chemical interactions. To date, numerous studies have been carried out on heavy metal ion sequestration using MXenes.

Among the various toxic heavy metal ions in water, Pb(II) is one of the most commonly encountered pollutants and its content in drinking water is strictly limited. In 2014, the $Ti_3C_2(OH/ONa)_xF_{2-x}$ MXene material[43] prepared *via* chemical exfoliation followed by alkalization intercalation was first reported to exhibit strong Pb(II) ion adsorption with a large uptake capacity (140 mg g^{-1}) and high selectivity even when other competing cations such as Ca(II) and Mg(II) coexist at high levels. The intercalation of cations or small organic molecules can increase the distance of the interlayers of MXene and enhance the interaction between the surface functional groups and MXene layers, and therefore helps the adsorption process. Especially, after purification with the applied management of 4500 kg water per kg alk-MXene, the effluent Pb(II) content can reach as low as 2 μg L^{-1}, which is below the drinking water standard set by the World Health Organization (10 μg L^{-1}). The adsorption mechanism was elucidated to be Pb(II) ions being trapped within hydroxyl potential traps, forming strong bonds between Pb and oxygen atoms (hydroxyls losing H atoms), as shown in Fig. 3. First-principles calculations revealed that different hydroxyl sites and different functional groups have a great influence on the adsorption behaviors of $Ti_3C_2(OH)_xF_{2-x}$ MXene for Pb(II) ions:[44] the hydroxyl group vertical to the titanium atom shows a stronger trend of removing ions than other adsorption structures, and the terminated F occupation of alk-MXene decreases the efficiency of the adsorption while the intercalation of Li, Na, and K atoms accelerates it. DFT studies of the adsorption behaviors of Pb on different MXenes in the general form of $M_2X(OH)_2$ (M = Sc, Ti, V, Cr, Zr, Nb, Mo, Hf, Ta, and X = C or N)[45] indicate that nitrides are basically more favorable for Pb ion adsorption than their carbide counterparts due to the different valence electron numbers between C and N atoms. In addition, $Sc_2C(OH)_2$ and $Zr_2C(OH)_2$ MXenes cannot be used for Pb removal. The weak ability of these two MXenes for Pb removal is mainly attributed to the energy difference between the sides of the adsorption reaction equation, *i.e.*, the adsorption structures have positive formation energies.

After Pb(II), Cr(VI) is listed as another important heavy metal pollutant in water, and its adsorption behavior on MXenes has also been investigated. Cr(VI) exists in the anionic form, *i.e.*, $Cr_2O_7^{2-}$. Ying *et al.* reported that $Ti_3C_2T_x$ MXene shows a high Cr(VI) adsorption capacity of 250 mg g^{-1} under optimized synthetic conditions (10% HF delamination, room temperature, pH = 5), and the residual concentration of Cr(VI) in the treated water is less than 5 ppm.[46] This MXene not only removes Cr(VI) by reducing Cr(VI) to the less toxic Cr(III), but also adsorbs the reduced Cr(III) simultaneously. The initial adsorption of Cr(VI) on $Ti_3C_2T_x$ is due to the electrostatic attraction between the positively charged surface of MXene and negatively charged $Cr_2O_7^{2-}$ (at low pH, the hydroxyl groups on the surface of $Ti_3C_2T_x$ MXene will be protonated). After adsorption, electrons are transferred from $Ti_3C_2T_x$ to $Cr_2O_7^{2-}$ with the assistance of H^+, producing TiO_2 and Cr(III) ions. The produced Cr(III) ions then interact with the [Ti–O] bond on the MXene and form the Ti–O–Cr(III) structure. Based on the reduction mechanism, it is confirmed that other oxidizing agents such as $K_3[Fe(CN)_6]$, $KMnO_4$, and $NaAuCl_4$ can also be reduced to low oxidation states and removed by $Ti_3C_2T_x$ MXene. By the *in situ* phase transformation of $Ti_3C_2(OH)_{0.8}F_{1.2}$ MXene under $FeCl_3$ conditions, an urchin-like rutile TiO_2–C nanocomposite with an abundance of (110) facets was fabricated, which displays a much higher Cr(VI) adsorption capacity of 225 mg g^{-1} than that of primitive $Ti_3C_2(OH)_{0.8}F_{1.2}$ MXene (~62 mg g^{-1}).[47] Theoretical calculation revealed that the adsorption energies of all three types of Cr(VI) ions (including CrO_4^{2-}, $HCrO_4^-$, and $Cr_2O_7^{2-}$ ions) on rutile TiO_2 are greater than that of water molecules, indicating that Cr(VI) ions can be adsorbed on rutile TiO_2 surfaces in aqueous solution. After adsorption, the

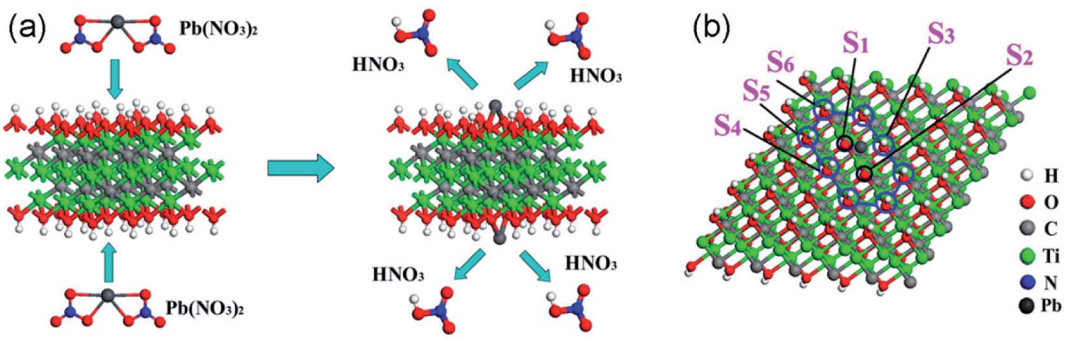

Fig. 3 (a) Schematic illustration of the formation of the $Ti_3C_2(O_2H_{2-2m}Pb_m)$ structure from $Ti_3C_2(OH)_2$ to $Ti_3C_2(O_2H_{2-2m}Pb_m)$; (b) top-view of the $Ti_3C_2(O_2H_{2-2m}Pb_m)$ structure when the Pb coverage is 1/9 ML. S1–S6 represent the different atom sites of the hydroxyl. Reprinted from ref. 44 with permission. Copyright 2015 American Chemical Society.

bridging oxo groups in Cr(VI) ions can further inhibit the adsorption of H_2O molecules on the rutile TiO_2 surfaces.

Besides Pb and Cr ions, first-principles calculations show that alkaline intercalated Ti_3C_2 MXene can also effectively remove a series of other heavy metal ions including Cu, Zn, Pd, and Cd, with formation energies ranging from −1.0 to −3.3 eV.[44] The general chemical reaction of heavy metals Y (in nitrate form) uptake on alk-MXene can be written as $Ti_3C_2(OH)_2 + mY(NO_3)_2 \rightarrow Ti_3C_2(O_2H_{2-2m}Y_m)_2 + 2mHNO_3$. The calculated formation energies of $Ti_3C_2(O_2H_{2-2m}Y_m)_2$ range from −1.0 to −3.3 eV for the Cu, Zn, Pd, and Cd elements. $Ti_3C_2T_x$ MXene also acts as an effective adsorbent for Ba(II)[48] and Cu(II) ions[49] (two typical pollutants in water), and also applied in experiment. The formation of both Ba–O and Ba–F bonds is found to contribute to the Ba(II) ion adsorption process. The maximum adsorption capacity is found experimentally to be 9.3 mg g^{-1} for an initial barium concentration of 55 ppm, which is higher than that of other competitors such as activated carbon and carbon nanotubes. Furthermore, the removal efficiency can reach up to 100% under optimized conditions. Since other studies[43] reported that –F groups hinder the adsorption of metal ions, more accurate investigations may be needed to clarify the effects of –F groups on the adsorption process. Regarding Cu(II) ions, the adsorption mechanism of ion exchange between the positively charged Cu ions and negatively charged terminal groups (–O and –OH) on the $Ti_3C_2T_x$ surface was experimentally confirmed. After the ion exchange, a further oxidation-reduction reaction occurs, resulting in the formation of rutile TiO_2 nanoparticles. The maximum Cu ion adsorption capacity of delaminated $Ti_3C_2T_x$ was experimentally determined to be 78.45 mg g^{-1}.

In addition to these ionic pollutants in water, MXenes have also shown strong adsorption capacity for free non-ionic metal atoms, and thus can be used as carriers for transition metal catalysts. Guo *et al.* studied the non-ionic Pb atom adsorption behaviors of different MXenes (including Ti_3C_2, V_2C_1 and Ti_2C_1) with different functional groups (including bare, H, OH, and F), and found that all the MXenes can effectively adsorb Pb atoms with a binding energy larger than 1 eV, except the F terminated ones.[50] The theoretical Pb adsorption capacity was calculated to be as high as 2560 mg g^{-1} for bare Ti_2C MXene and 1280 mg g^{-1} for H-terminated Ti_2C MXene. They also found the bare and OH terminated MXenes of the three types show a high adsorption capability for Cu atoms. Yang *et al.* also predicted that $Ti_2C(OH)_2$ and $Ti_3C_2(OH)_2$ MXene can effectively adsorb free non-ionic Au atoms with a high adsorption energy larger than 3 eV, and the O and F groups significantly reduce the adsorption ability.[51] Since free non-ionic Pb, Cu and Au atoms are hard to obtain under common conditions, these studies may require future experimental validation.

Besides adsorptive removal, MXene materials can also be applied for sensing trace amounts of heavy metal ions. An alk-Ti_3C_2 modified glassy carbon electrode is reported to exhibit a highly sensitive electrochemical response to Cd(II), Pb(II), Cu(II) and Hg(II) ions using square-wave anodic stripping voltammetry.[52] Under optimized conditions, the electrode displays a detection limit of 0.098 μM, 0.041 μM, 0.032 μM and 0.130 μM for Cd(II), Pb(II), Cu(II) and Hg(II), respectively, which is superior to most of the state-of-the-art sensors. Moreover, the peak potentials of each heavy metal are well defined and sufficiently separated during the simultaneous voltammetric determination of four target heavy metal ions, which is very suitable for the simultaneous and selective detection of co-existing metal ions.

Overall, MXenes show strong adsorption capabilities for metal ions and non-ionic atoms, which are even stronger than that of carbon nanotubes and graphene oxide,[17–19] even if the atomic weight of the carbon element is usually much lower than transition metal elements in MXenes (for example, the typical Pb(II) uptake capacity of oxidized carbon nanotubes is below 100 mg g^{-1}). These unique adsorption properties are generally attributed to the natural surface-functionalization of MXenes during the synthetic process using acidic fluoride-containing solutions.

3.2 Organic dye adsorption

Organic dyes are also an important type of pollutant in water. Dyes usually have a stable molecular structure and are difficult to biodegrade. The presence of dyes in water can directly impact the ecosystem and even the health of human beings through the contamination of drinking water supplies. Dyes usually exist in the form of cations or anions in water, and thus can be adsorbed by specific adsorbents. Several groups have investigated the possibility of removing organic dye pollutants using MXene materials, especially combined with the UV photocatalytic technique to further degrade them.

The charged state of a dye is a critical factor to its adsorption on MXenes. Studies of the adsorptive properties of the cationic dye methylene blue (MB) and anionic dye acid blue 80 (AB80) on $Ti_3C_2T_x$ MXene[53] reveal that MB can be strongly and irreversibly bonded to $Ti_3C_2T_x$ (with the adsorption capacity of ~39 mg g^{-1}), while AB80 can hardly adsorb on MXene. The preferential adsorption of the cationic dye over anionic dye is attributed to the electrostatic interactions between the positively charged dye cations and the negatively charged surfaces of MXenes in aqueous solution. UV light is also found to significantly enhance the degradation rate of MB and AB80 dye in solutions containing both the dye and $Ti_3C_2T_x$ MXene. Similar to Pb ion adsorption,[43] expanding the interlayer spacing of MXene is also an efficient approach to improve its dye adsorption performance. Zheng *et al.* reported that the interlayer spacing of $Ti_3C_2T_x$ MXene can be increased by up to 29% *via* LiOH treatment and 28% *via* NaOH treatment.[54] The adsorption capacity of LiOH–$Ti_3C_2T_x$ and NaOH–$Ti_3C_2T_x$ for MB reaches 121 mg g^{-1} and 189 mg g^{-1}, respectively, in comparison with that of the pristine $Ti_3C_2T_x$ MXene without alkaline treatment (100 mg g^{-1}).

Semiconductor/MXene nanocomposites have also been studied to enhance photocatalytic activity. Gao *et al.* synthesized TiO_2/Ti_3C_2 nanocomposites *via* a hydrothermal process,[55] which showed improved photocatalytic activity for methyl orange degradation under ultraviolet light irradiation compared to simplex TiO_2 or Ti_3C_2. Their studies suggested that the TiO_2/Ti_3C_2 composite exhibits more effective electron–hole

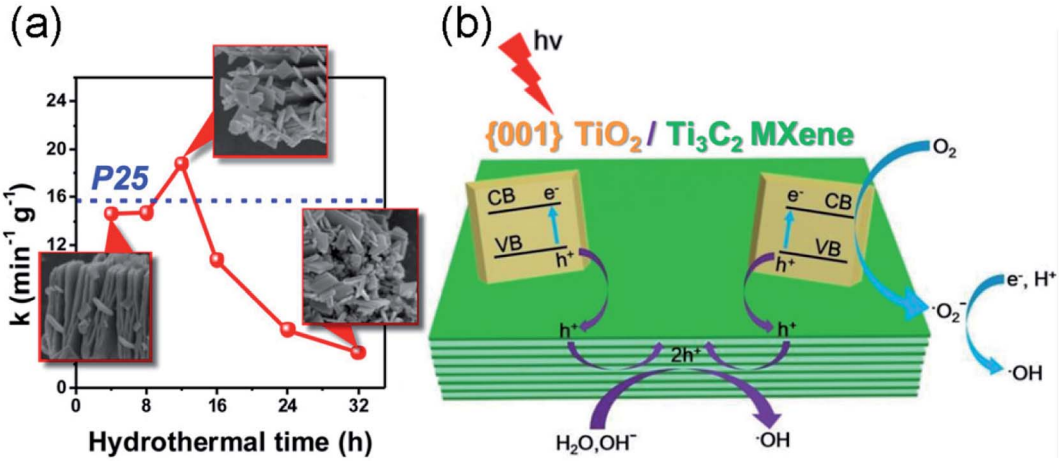

Fig. 4 (a) Photocatalytic degradation rate constant (k) of (001)TiO_2/Ti_3C_2 prepared for different hydrothermal times. (b) Schematic illustration of the charge-transfer process over (001)TiO_2/Ti_3C_2. Reprinted from ref. 56 with permission. Copyright 2016 American Chemical Society.

separation than pure TiO_2 or Ti_3C_2 under UV irradiation. To further improve the photocatalytic activity of the TiO_2/Ti_3C_2 complex, Peng *et al.* synthesized a hybrid comprised of (001) facets of TiO_2 nanosheets and layered Ti_3C_2 *via* the facile *in situ* hydrothermal partial oxidation of Ti_3C_2.[56] The catalytic activity is highly dependent on the hydrothermal time (Fig. 4a). The unique hybrid significantly enhances the photocatalytic degradation of methyl orange dye. The result was attributed to the fact that the highly active (001) facets of TiO_2 allow the high-efficiency photogeneration of electron–hole pairs, which are substantially promoted by the hole trapping effect by the interfacial Schottky junction with 2D Ti_3C_2 acting as a reservoir of holes, as illustrated in Fig. 4b. This design not only allows for high-efficiency separation of electron–hole pairs, but also overcomes the problem of their rapid recombination. Zhou *et al.* synthesized a CeO_2/Ti_3C_2 nanocomposite *via* a one-step hydrothermal method based on the electrostatic attraction between Ce^{3+} ions and Ti_3C_2 nanosheets.[57] The composite shows excellent photocatalytic activity toward the degradation of Rhodamine B compared with pure Ti_3C_2 and CeO_2, which is attributed to the enhanced utilization of solar energy.

From the above literature, two basic conclusions can be derived, the adsorption mechanism of dyes on MXenes is electrostatic attraction and semiconductor/MXene nanocomposites are an effective approach for the photocatalytic degradation of dyes compared to their simplex component counterparts.

3.3 Radionuclide pollutant adsorption

With the rapid development of the nuclear industry and the peaceful utilization of nuclear energy, nuclear waste pollution has become a challenging environmental concern. As is known, the contamination of some long-lived actinides can be a significant hazard even at trace amount due to their long-term radiological and chemical toxicities. The unique characteristics of MXenes such as high ability to resist strong radiation and good chemical compatibility with molten salt harsh materials give them the potential to clean up radionuclides for nuclear waste treatment.

Using multi-layered vanadium carbide V_2CT_x nanosheets as a case study, MXenes have been shown to be competitive inorganic adsorbents for actinide capture from aqueous solution.[58,59] Uranium, which normally exists as UO_2^{2+} in most processing and environmental conditions, is one of the most important radionuclides due to its central role in the nuclear energy industry and its relative enrichment in nature. It is confirmed that V_2CT_x MXene can adsorb uranium U(VI) with a high uptake capacity of 174 mg g^{-1}, along with fast sorption kinetics and desirable selectivity.[58] Density functional theory calculations in combination with X-ray absorption fine structure characterization suggest that uranyl ions prefer to coordinate with hydroxyl groups bonded to the V sites of MXene *via* the formation of bidentate inner-sphere complexes, as shown in Fig. 5. According to the uranium speciation diagram, uranium ions can exist with different ligands such as aqueous, carbonate and hydroxylated species. To specify the adsorption behaviors of uranium on MXene, the adsorption properties of hydroxylated V_2C nanosheets for uranyl ions with different ligands in the general form $[UO_2(L_1)_x(L_2)_y(L_3)_z]^n$ (where, L_1, L_2 and L_3 stand for H_2O, OH and CO_3, respectively)[59] are further clarified. All uranyl species can bond strongly with $V_2C(OH)_2$ nanosheets with high adsorption energies greater than 3 eV. Among the studied uranyl species, aquouranyl $[UO_2(H_2O)_5]^{2+}$ bonds the strongest to the hydroxylated V_2C nanosheet. It is also found that the terminated –F groups on the V_2C nanosheets can weaken the adsorption capability for uranyl ions.

Titanium carbide $Ti_3C_2T_x$, as the typical material of MXene, with the merits of good development and inexpensive preparation, is the ideal adsorbent for radionuclide elimination with respect to technology and the economy. DFT studies of the adsorption behaviors of U(VI) ions on $Ti_3C_2(OH)_2$ MXene[60] have shown that U(VI) ions can form strong bonds with MXene in aqueous solution regardless of the presence of anionic ligands such as OH^-, Cl^- and NO_3^-. Chemical interactions and

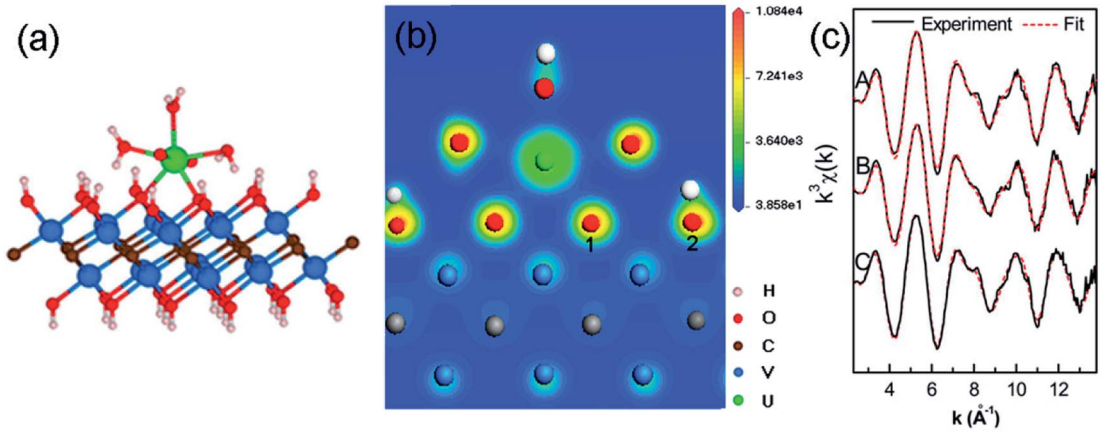

Fig. 5 Adsorption configuration of a U ion on V_2CT_x nanosheets as analyzed by DFT and X-ray adsorption spectroscopic approaches. (a) Bidentate inner-sphere adsorption configuration of a uranium ion on V_2CT_x nanosheets, (b) charge density distribution of the adsorption structure by DFT simulations, (c) raw U L_{III}-edge k^3-weighted extended X-ray absorption fine structure (EXAFS) spectra and the best theoretical fits of U adsorbed on V_2CT_x nanosheets under different conditions. Reprinted from ref. 58 with permission. Copyright 2015 and 2016 American Chemical Society.

hydrogen bonds are considered as the main adsorption interactions. Based on the stable adsorption configuration, the theoretical adsorption capacity can approach 595.3 mg g^{-1} for the $[UO_2(H_2O)_5]^{2+}$ species.

In experiment, a major challenge for radionuclide removal using $Ti_3C_2T_x$ as the adsorbent material is the contradiction between the small interlayer space of $Ti_3C_2T_x$ MXene and the large hydrated radionuclide ionic radius, which limits the radionuclide adsorption capacity. Delamination of multilayered $Ti_3C_2T_x$ into nanoflakes is an ideal approach to significantly improve the adsorption capacity. Furthermore, hydration is found to be an effective method to enhance the adsorption properties of U(VI) ions on MXenes.[61] Through this approach, the presence of hydrophilic groups and van der Waals weak interactions can increase the interlayered distance of MXenes, and therefore enhance their adsorption capacity for U ions.

Briefly, MXene materials have been demonstrated to be effective adsorbents for uranium ions both experimentally and theoretically. Chemical interactions and hydrogen bonds are the main adsorption mechanism. Except for uranium, the adsorption of other radionuclide ions (*e.g.*, Np and Pu ions) on MXenes are still unknown and need further investigation.

3.4 Gaseous contaminant adsorption

Gaseous contaminants mainly include toxic inorganic gases (NO_x, SO_x, H_2S, NH_3, and CO), and volatile organic compounds (VOCs), most of which can cause serious diseases to humans and other living organisms. Thus, both effectively sensing and removing them are of high importance. A number of studies have been carried out on gaseous contaminant adsorption using MXenes.

Regarding inorganic gases, first-principles calculations of the adsorption behaviors of NH_3, H_2, CH_4, CO, CO_2, N_2, NO_2 and O_2 on monolayer Ti_2CO_2 reveal that only NH_3 can be chemisorbed on Ti_2CO_2 (adsorption energy of −0.37 eV), while the others are physisorbed on Ti_2CO_2 with low adsorption energies, as shown in Fig. 6a[62]. The electrical conductivity of Ti_2CO_2 changes significantly after the adsorption of NH_3, indicating that Ti_2CO_2 can be a potential NH_3 sensor with high sensitivity (Fig. 6b). Additionally, the interaction between NH_3 and Ti_2CO_2 can be further enhanced by applying strain on the nanosheet. The adsorption behavior of NH_3 on a series of O-terminated semiconducting MXenes with the general form M_2CO_2 (M = Sc, Ti, Zr, and Hf) were investigated using first-principles simulations.[63] All the studied MXenes can chemisorb NH_3 with notable charge transfer. The adsorbed NH_3 can be further released from the MXenes by injecting electrons into them. These results indicate that M_2CO_2 MXenes are very suitable as NH_3 sensors. The density functional theory investigations by Morales-Garcia *et al.* showed that bare M_2C (M = Ti, Zr, Hf, V, Nb, Ta, Cr, Mo, and W) MXenes without surface functional groups can effectively adsorb CO_2 even at low CO_2 partial pressures and high temperatures, and thus can act as very promising candidates for carbon dioxide capture, storage, and activation.[64]

Besides the adsorption of inorganic gaseous contaminants, MXene materials can also be utilized to fabricate gas sensors for VOCs. Kim *et al.* reported that $Ti_3C_2T_x$ MXene exhibits a very low detection limit of 50–100 ppb for VOC gases (including acetone, ethanol, and propanal) and ammonia at room temperature.[65] The high metallic conductivity and fully functionalized surface of $Ti_3C_2T_x$ MXene lead to an ultrahigh signal-to-noise ratio, which is superior to conventional semiconductor channel materials and other well-known 2D materials (*e.g.*, MoS_2). The terminal hydroxyl (–OH) groups on the surface of $Ti_3C_2T_x$ are mainly responsible for the adsorptive detection of the target species.

3.5 Adsorption of other pollutants

In addition to the abovementioned pollutants, the adsorption of some other pollutants have also been demonstrated using MXene materials due to their active surface structures.

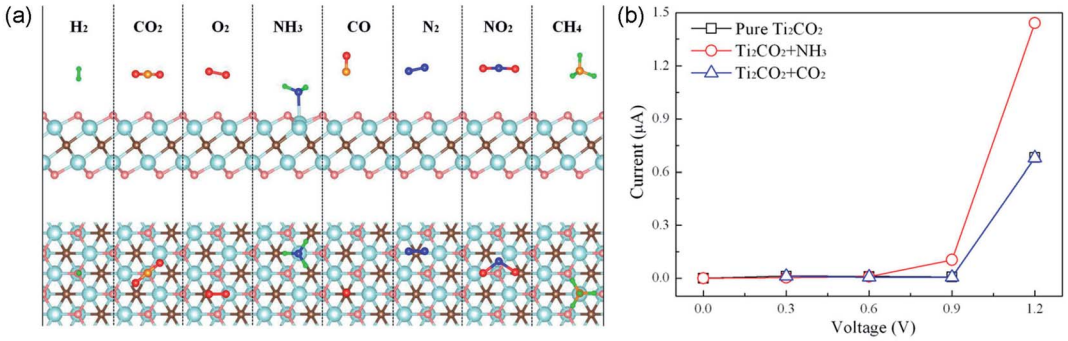

Fig. 6 (a) Schematic illustration of the adsorption of NH_3, H_2, CH_4, CO, CO_2, N_2, NO_2 and O_2 molecules on monolayer Ti_2CO_2. (b) Current–voltage relationship before and after the adsorption of NH_3 or CO_2 molecule on monolayer Ti_2CO_2. Reprinted from ref. 62 with permission. Copyright 2015 American Chemical Society.

Zhang *et al.* synthesized a novel sandwiched MXene-iron oxide (MXI) 2D material by selectively exfoliating an Al layer followed by magnetic ferric oxide intercalation for phosphate sequestration in water.[66] Compared with commercial adsorbents, the MXI nanocomposite exhibits superior treatment capacities (2100 kg and 2400 kg kg^{-1} sorbent in simulated and real phosphate wastewater tests, respectively), with fast kinetics. The grown ultrafine nano-Fe_2O_3 particles intercalate into the interior layers of MXene, releasing the overlapped layers and further forming Ti–OH terminated layered surface within the MXene and Fe–OH exchanged sites of ferric oxide, and contribute to the unique phosphate sequestration behaviors. Additionally, after phosphate adsorption, the material can be recycled using binary alkaline brine solutions. Wu *et al.* fabricated an electrochemical tyrosinase biosensor based on the $Ti_3C_2T_x$ MXene material, which demonstrates good repeatability and reproducibility, long-term stability and high recovery for the detection of phenol in water.[67] The adsorption mechanism involves the oxidation–reduction of phenol by the tyrosinase biosensor.

For clarity, the specific uptake capacities of MXenes and their derivatives for several pollutants are listed in Table 1.

Besides adsorption, MXene materials can also be fabricated into a membrane form and used as a sieve for the filtration of pollutant species in wastewater. Ren *et al.* fabricated $Ti_3C_2T_x$ membranes using a vacuum filtration method and conducted permeation tests for a series of cations.[68] Their results revealed that the separation properties of the membranes are highly dependent on the size and charge of the cations, where, the permeation of cations decreases with an increase in size and charge, and cations with hydration radii larger than the interlayer spacing are nonpermeable (*e.g.* methylene blue ions). The $Ti_3C_2T_x$ membranes demonstrated a better performance than graphene oxide in the separation of higher charged cations under the same test conditions. The hydrophilic nature of $Ti_3C_2T_x$ accompanied by the presence of H_2O between the layers is attributed to the ultrafast water flux of 37.4 L (bar h $m^2)^{-1}$. Ding *et al.* fabricated $Ti_3C_2T_x$ membranes with expanded microchannels to further increase the water flux.[69] During the fabrication process, colloidal $Fe(OH)_3$ was employed as the intercalation medium to increase the interlayer spacing. The resulting $Ti_3C_2T_x$ membranes exhibited an excellent water permeation performance (higher than 1000 L (bar h $m^2)^{-1}$) with a favorable rejection rate (over 90%) for Evans blue molecules. Berdiyorov *et al.* investigated the mechanism of the charge-selective permeation property of $Ti_3C_2(OH)_2$ MXene using first-principles density functional theory.[70] They found that this phenomenon originates from the charged nature of the MXene layers, where, ions with different charge states have different energy barriers for the intercalation between the MXene layers due to electrostatic interactions. The calculated energy barriers are 0.14 eV, 0.26 eV, and 0.34 eV for Na^+, Mg^{2+}, and Al^{3+}, respectively.

4 Summary and outlook

In summary, 2D transition metal carbides/nitrides, *i.e.* MXenes, have demonstrated very promising results in the adsorptive remediation of polar and ionic pollutants, including heavy metal ions, organic dyes, radionuclides and gaseous pollutants. Their overall performances seem better than that of conventional pollutant adsorbents and even other low-dimensional materials, such as carbon nanotubes and graphene. Nevertheless, there are still many open questions that need to be addressed before these materials can be used practically.

Although theoretical simulations have predicted a large number of MXene materials, the number of the experimentally synthesized MXenes is limited. For example, calculations have shown that Hf_2CO_2 MXene possesses excellent thermal and electrical properties to be a promising semiconductor,[55] but it is yet to be synthesized experimentally. Thus, the synthesis of the large number of MXenes becomes an important research direction. We expect there are still many MXenes that are more suitable as adsorbents, and worth investigating. Comparative studies between the properties of the newly obtained and readily available MXenes should be conducted.

Apparently, the functional groups on the surfaces and delamination conditions of MXenes are strongly related to their adsorption capabilities (in fact, also to most other chemical properties). Large discrepancies are often found between the theoretical and experimental uptake capacities, which are generally attributed to non-ideal surface conditions (*e.g.* ref. 58).

Table 1 Specific uptake capacities of MXenes and their derivatives for several pollutants

MXene or derivative	Pollutant	Uptake capacity	Reference
$Ti_3C_2(OH/ONa)_xF_{2-x}$	Pb(II)	140 mg g^{-1}	43
$Ti_3C_2T_x$	Cr(VI)	250 mg g^{-1}	46
$Ti_3C_2(OH)_{0.8}F_{1.2}$	Cr(VI)	62 mg g^{-1}	47
TiO_2–C nanocomposite	Cr(VI)	225 mg g^{-1}	47
$Ti_3C_2T_x$	Ba(II)	9.3 mg g^{-1} (for initial barium concentration of 55 ppm)	48
$Ti_3C_2T_x$	Cu(II)	78.45 mg g^{-1}	49
$Ti_3C_2T_x$	Methylene blue	39 mg g^{-1}	53
$Ti_3C_2T_x$	Methylene blue	100 mg g^{-1}	54
LiOH–$Ti_3C_2T_x$	Methylene blue	121 mg g^{-1}	54
NaOH–$Ti_3C_2T_x$	Methylene blue	189 mg g^{-1}	54
V_2CT_x	U(VI)	174 mg g^{-1}	58
$V_2C(OH)_2$	U(VI)	536 mg g^{-1} (theoretical)	58
Ti_2C	Pb	2560 mg g^{-1} (theoretical)	45
Ti_2CH_2	Pb	1280 mg g^{-1} (theoretical)	45
$Ti_3C_2(OH)_2$	U(VI)	595.3 mg g^{-1} (theoretical for $[UO_2(H_2O)_5]^{2+}$)	60
M_2C (M = Ti, Zr, Hf, V, CO_2, Nb, Ta, Cr, Mo, and W)		103–363 mg g^{-1} (theoretical)	64

Therefore, the development of new synthetic procedures and post treatments to achieve uniform functional groups (such as hydroxyl, fluorine or oxygen) and full delamination are highly necessary. Non-terminated MXenes, the surfaces of which are comprised of metal atoms, are considered highly reactive,[45] and thus need to be further studied for adsorption applications, especially experimentally.

Since it is reported that $Ti_3C_2T_x$ MXene can be oxidized to titania over a long period in water,[53] the stability of MXene materials needs to be critically considered when used as adsorbents, especially in water. Therefore, the stability of various MXenes in water together with their adsorption capacities are highly worth investigating. Highly stable and strongly adsorptive MXenes are desirable in practical applications.

Toxicity is a significant issue in all applications. It is very recently reported that delaminated Ti_3C_2 MXene has effects on the viability of both normal and cancerous cells.[70] Although this is not an exciting result, deeper investigations on the toxicity of MXenes are needed.

To evaluate the reliability and lifespan of recycled MXenes used as adsorbent materials, more careful investigations are still required. Especially, clarification of the exact mechanism of the decline in performance after repeated use is of high importance for practical applications.

Conflicts of interest

There are no conflicts to declare.

Acknowledgements

This work was supported by the National Natural Science Foundation of China (Grant No. 11505006, 11675192) and Beijing Natural Science Foundation (Grant No. 2182042), and Zhengzhou Ruitai Refractory Technology Co. Ltd, China.

References

1 G. F. Vandegrift, D. T. Reed and I. R. Tasker, *Environmental Remediation: Removing Organic and Metal Ion Pollutants*, ACS Publications, 1992.
2 B. Gu, Y. Ku and P. M. Jardine, *Environ. Sci. Technol.*, 2004, **38**, 3184–3188.
3 Q. Zhang, N. Wang, L. Zhao, T. Xu and Y. Cheng, *ACS Appl. Mater. Interfaces*, 2013, **5**, 1907–1912.
4 F. Fu, L. Xie, B. Tang, Q. Wang and S. Jiang, *Chem. Eng. J.*, 2012, **189**, 283–287.
5 S. Kerisit and C. Liu, *Environ. Sci. Technol.*, 2014, **48**, 3899–3907.
6 K. Y. Foo and B. H. Hameed, *J. Hazard. Mater.*, 2010, **175**, 1–11.
7 S. S. Gupta and K. G. Bhattacharyya, *Phys. Chem. Chem. Phys.*, 2012, **14**, 6698–6723.
8 S. Wang and Y. Peng, *Chem. Eng. J.*, 2010, **156**, 11–24.
9 W. W. Ngah, L. C. Teong and M. Hanafiah, *Carbohydr. Polym.*, 2011, **83**, 1446–1456.
10 A. A. Adeyemo, I. O. Adeoye and O. S. Bello, *Toxicol. Environ. Chem.*, 2012, **94**, 1846–1863.
11 L. Yuan, M. Tian, J. Lan, X. Cao, X. Wang, Z. Chai, J. Gibson and W. Shi, *Chem. Commun.*, 2018, **54**, 370–373.
12 K. S. Novoselov, A. K. Geim, S. V. Morozov, D. Jiang, Y. Zhang, S. V. Dubonos, I. V. Grigorieva and A. A. Firsov, *Science*, 2004, **306**, 666–669.
13 K. S. Novoselov, A. K. Geim, S. Morozov, D. Jiang, M. Katsnelson, I. Grigorieva, S. Dubonos and A. A. Firsov, *Nature*, 2005, **438**, 197–200.
14 J. N. Coleman, M. Lotya, A. O Neill, S. D. Bergin, P. J. King, U. Khan, K. Young, A. Gaucher, S. De and R. J. Smith, *Science*, 2011, **331**, 568–571.
15 R. Ma and T. Sasaki, *Adv. Mater.*, 2010, **22**, 5082–5104.

16 L. Yuan, Z. Bai, R. Zhao, Y. Liu, Z. Li, S. Chu, L. Zheng, J. Zhang, Y. Zhao and Z. Chai, *ACS Appl. Mater. Interfaces*, 2014, **6**, 4786–4796.
17 K. V. Wong and B. Bachelier, *J. Energy Resour. Technol.*, 2014, **136**, 021601.
18 F. Perreault, A. F. De Faria and M. Elimelech, *Chem. Soc. Rev.*, 2015, **44**, 5861–5896.
19 S. Wang, H. Sun, H. Ang and M. O. Tadé, *Chem. Eng. J.*, 2013, **226**, 336–347.
20 O. Chen, Y. Lin, W. Cao and C. Chang, *Mater. Lett.*, 2017, **190**, 280–282.
21 M. Naguib, M. Kurtoglu, V. Presser, J. Lu, J. Niu, M. Heon, L. Hultman, Y. Gogotsi and M. W. Barsoum, *Adv. Mater.*, 2011, **23**, 4248–4253.
22 M. Naguib, V. N. Mochalin, M. W. Barsoum and Y. Gogotsi, *Adv. Mater.*, 2014, **26**, 992–1005.
23 M. Naguib, O. Mashtalir, J. Carle, V. Presser, J. Lu, L. Hultman, Y. Gogotsi and M. W. Barsoum, *ACS Nano*, 2012, **6**, 1322–1331.
24 M. Khazaei, M. Arai, T. Sasaki, C. Y. Chung, N. S. Venkataramanan, M. Estili, Y. Sakka and Y. Kawazoe, *Adv. Funct. Mater.*, 2013, **23**, 2185–2192.
25 B. Anasori, Y. Xie, M. Beidaghi, J. Lu, B. C. Hosler, L. Hultman, P. R. Kent, Y. Gogotsi and M. W. Barsoum, *ACS Nano*, 2015, **9**, 9507–9516.
26 M. Ghidiu, M. R. Lukatskaya, M. Zhao, Y. Gogotsi and M. W. Barsoum, *Nature*, 2014, **516**, 78–81.
27 Y. Lee, S. B. Cho and Y. Chung, *ACS Appl. Mater. Interfaces*, 2014, **6**, 14724–14728.
28 J. Guo, Y. Sun, B. Liu, Q. Zhang and Q. Peng, *J. Alloys Compd.*, 2017, **712**, 752–759.
29 Q. Hu, D. Sun, Q. Wu, H. Wang, L. Wang, B. Liu, A. Zhou and J. He, *J. Phys. Chem. A*, 2013, **117**, 14253–14260.
30 M. R. Lukatskaya, O. Mashtalir, C. E. Ren, Y. Dall Agnese, P. Rozier, P. L. Taberna, M. Naguib, P. Simon, M. W. Barsoum and Y. Gogotsi, *Science*, 2013, **341**, 1502–1505.
31 B. Anasori, M. R. Lukatskaya and Y. Gogotsi, *Nat. Rev. Mater.*, 2017, **2**, 16098.
32 J. Lei, X. Zhang and Z. Zhou, *Front. Phys.*, 2015, **10**, 276–286.
33 M. Ashton, R. G. Hennig and S. B. Sinnott, *Appl. Phys. Lett.*, 2016, **108**, 023901.
34 V. M. H. Ng, H. Huang, K. Zhou, P. S. Lee, W. Que, J. Z. Xu and L. B. Kong, *J. Mater. Chem. A*, 2017, **5**, 3039–3068.
35 J. Zhou, X. Zha, F. Y. Chen, Q. Ye, P. Eklund, S. Du and Q. Huang, *Angew. Chem., Int. Ed.*, 2016, **128**, 5092–5097.
36 J. Zhou, X. Zha, X. Zhou, F. Chen, G. Gao, S. Wang, C. Shen, T. Chen, C. Zhi and P. Eklund, *ACS Nano*, 2017, **11**, 3841–3850.
37 X. Wang, C. Garnero, G. Rochard, D. Magne, S. Morisset, S. Hurand, P. Chartier, J. Rousseau, T. Cabioc'H and C. Coutanceau, *J. Mater. Chem. A*, 2017, **5**, 22012–22023.
38 M. A. Hope, A. C. Forse, K. J. Griffith, M. R. Lukatskaya, M. Ghidiu, Y. Gogotsi and C. P. Grey, *Phys. Chem. Chem. Phys.*, 2016, **18**, 5099–5102.
39 H. Wang, M. Naguib, K. Page, D. J. Wesolowski and Y. Gogotsi, *Chem. Mater.*, 2015, **28**, 349–359.
40 Y. Xie, M. Naguib, V. N. Mochalin, M. W. Barsoum, Y. Gogotsi, X. Yu, K. Nam, X. Yang, A. I. Kolesnikov and P. R. Kent, *J. Am. Chem. Soc.*, 2014, **136**, 6385–6394.
41 C. Xu, L. Wang, Z. Liu, L. Chen, J. Guo, N. Kang, X. Ma, H. Cheng and W. Ren, *Nat. Mater.*, 2015, **14**, 1135.
42 X. Zha, J. Yin, Y. Zhou, Q. Huang, K. Luo, J. Lang, J. S. Francisco, J. He and S. Du, *J. Phys. Chem. C*, 2016, **120**, 15082–15088.
43 Q. Peng, J. Guo, Q. Zhang, J. Xiang, B. Liu, A. Zhou, R. Liu and Y. Tian, *J. Am. Chem. Soc.*, 2014, **136**, 4113–4116.
44 J. Guo, Q. Peng, H. Fu, G. Zou and Q. Zhang, *J. Phys. Chem. C*, 2015, **119**, 20923–20930.
45 J. Guo, H. Fu, G. Zou, Q. Zhang, Z. Zhang and Q. Peng, *J. Alloys Compd.*, 2016, **684**, 504–509.
46 Y. Ying, Y. Liu, X. Wang, Y. Mao, W. Cao, P. Hu and X. Peng, *ACS Appl. Mater. Interfaces*, 2015, **7**, 1795–1803.
47 G. Zou, J. Guo, Q. Peng, A. Zhou, Q. Zhang and B. Liu, *J. Mater. Chem. A*, 2016, **4**, 489–499.
48 A. K. Fard, G. Mckay, R. Chamoun, T. Rhadfi, H. Preud'Homme and M. A. Atieh, *Chem. Eng. J.*, 2017, **317**, 331–342.
49 A. Shahzad, K. Rasool, W. Miran, M. Nawaz, J. Jang, K. Mahmoud and D. S. Lee, *ACS Sustainable Chem. Eng.*, 2017, **5**, 11481–11488.
50 X. Guo, X. Zhang, S. Zhao, Q. Huang and J. Xue, *Phys. Chem. Chem. Phys.*, 2016, **18**, 228–233.
51 J. Yang, S. Zhang, J. Ji and S. Wei, *Acta Phys.-Chim. Sin.*, 2015, **31**, 369–376.
52 X. Zhu, B. Liu, H. Hou, Z. Huang, K. M. Zeinu, L. Huang, X. Yuan, D. Guo, J. Hu and J. Yang, *Electrochim. Acta*, 2017, **248**, 46–57.
53 O. Mashtalir, K. M. Cook, V. N. Mochalin, M. Crowe, M. W. Barsoum and Y. Gogotsi, *J. Mater. Chem. A*, 2014, **2**, 14334–14338.
54 W. Zheng, P. Zhang, W. Tian, X. Qin, Y. Zhang and Z. M. Sun, *Mater. Chem. Phys.*, 2018, **206**, 270–276.
55 Y. Gao, L. Wang, A. Zhou, Z. Li, J. Chen, H. Bala, Q. Hu and X. Cao, *Mater. Lett.*, 2015, **150**, 62–64.
56 C. Peng, X. Yang, Y. Li, H. Yu, H. Wang and F. Peng, *ACS Appl. Mater. Interfaces*, 2016, **8**, 6051–6060.
57 W. Zhou, J. Zhu, F. Wang, M. Cao and T. Zhao, *Mater. Lett.*, 2017, **206**, 237–240.
58 L. Wang, L. Yuan, K. Chen, Y. Zhang, Q. Deng, S. Du, Q. Huang, L. Zheng, J. Zhang and Z. Chai, *ACS Appl. Mater. Interfaces*, 2016, **8**, 16396–16403.
59 Y. Zhang, Z. Zhou, J. Lan, C. Ge, Z. Chai, P. Zhang and W. Shi, *Appl. Surf. Sci.*, 2017, **426**, 572–578.
60 Y. Zhang, J. Lan, L. Wang, Q. Wu, C. Wang, T. Bo, Z. Chai and W. Shi, *J. Hazard. Mater.*, 2016, **308**, 402–410.
61 L. Wang, W. Tao, L. Yuan, Z. Liu, Q. Huang, Z. Chai, J. K. Gibson and W. Shi, *Chem. Commun.*, 2017, **53**, 12084–12087.
62 X. Yu, Y. Li, J. Cheng, Z. Liu, Q. Li, W. Li, X. Yang and B. Xiao, *ACS Appl. Mater. Interfaces*, 2015, **7**, 13707–13713.
63 B. Xiao, Y. Li, X. Yu and J. Cheng, *Sens. Actuators, B*, 2016, **235**, 103–109.

64 A. Morales-Garcia, A. F. Fernández, F. Viñes and F. Illas, *J. Mater. Chem. A*, 2018, **6**, 3381–3385.
65 S. J. Kim, H. J. Koh, C. E. Ren, O. Kwon, K. Maleski, S. Y. Cho, B. Anasori, C. K. Kim, Y. K. Choi and J. Kim, *ACS Nano*, 2018, **12**, 986–993.
66 Q. Zhang, J. Teng, G. Zou, Q. Peng, Q. Du, T. Jiao and J. Xiang, *Nanoscale*, 2016, **8**, 7085–7093.
67 L. Wu, X. Lu, Dhanjai, Z. S. Wu, Y. Dong, X. Wang, S. Zheng and J. Chen, *Biosens. Bioelectron.*, 2018, **107**, 69.
68 C. E. Ren, K. B. Hatzell, M. Alhabeb, Z. Ling, K. A. Mahmoud and Y. Gogotsi, *J. Phys. Chem. Lett.*, 2015, **6**, 4026–4031.
69 L. Ding, Y. Wei, Y. Wang, H. Chen, J. Caro and H. Wang, *Angew. Chem., Int. Ed.*, 2017, **56**, 1825–1829.
70 G. R. Berdiyorov, M. E. Madjet and K. A. Mahmoud, *Appl. Phys. Lett.*, 2016, **108**, 113110.
71 A. M. Jastrzębska, A. Szuplewska, T. Wojciechowski, M. Chudy, W. Ziemkowska, L. Chlubny, A. Rozmysłowska and A. Olszyna, *J. Hazard. Mater.*, 2017, **339**, 1–8.